Exploring the therapeutic potential of rabdoternin E in lung cancer treatment: Targeting the ROS/p38 MAPK/JNK signaling pathway

JINGHUI JIN[1*], JUAN NAN[1*], YANPO SI[1,2], XIAOHUI CHEN[2], HAIBO WANG[3], XIAOWEI WANG[3], JINGWANG HUANG[4] and TAO GUO[1]

[1]School of Pharmacy, Henan University of Chinese Medicine, Zhengzhou, Henan 450046, P.R. China; [2]Academy of Chinese Medical Science, Henan University of Chinese Medicine, Zhengzhou, Henan 450046, P.R. China; [3]NMPA Key Laboratory for Quality Control of Traditional Chinese Medicine (Chinese Materia Medica and Prepared Sections), Henan Institute for Drug and Medical Device Inspection (Henan Vaccine Issuance Center), Zhengzhou, Henan 450018, P.R. China; [4]Henan Jishi Pharmaceutical Co., Ltd., Jiyuan, Henan 459000, P.R. China

Received April 2, 2024; Accepted July 3, 2024

DOI: 10.3892/mmr.2024.13330

Abstract. Lung cancer has the highest incidence and mortality rates of all cancer types in China and therefore represents a serious threat to human health. In the present study, the mechanism of rabdoternin E against the proliferation of the lung cancer cell line A549 was explored. It was found that rabdoternin E caused the accumulation of large amounts of reactive oxygen species (ROS), promoted cell S phase arrest by reducing the expression of CDK2 and cyclin A2, induced apoptosis by increasing the Bax/Bcl-2 ratio and promoted the phosphorylation of proteins in the ROS/p38 MAPK/JNK signaling pathway, which is associated with apoptosis and ferroptosis. In addition, it was also found that Z-VAD-FMK (an apoptosis inhibitor), ferrostatin-1 (ferroptosis inhibitor) and N-acetylcysteine (a ROS inhibitor) could partially or greatly reverse the cytotoxicity of rabdoternin E to A549 cells. Similarly, NAC (N-acetylcysteine) treatment notably inhibited the rabdoternin E-stimulated p38 MAPK and JNK activation. Furthermore, *in vivo* experiments in mice revealed that Rabdoternin E markedly reduced tumor volume and weight and regulated the expression levels of apoptosis and ferroptosis-related proteins (including Ki67, Bcl-2, Bax, glutathione peroxidase 4, solute carrier family 7 member 11 and transferrin) in the tumor tissues of mice. Histopathological observation confirmed that the number of tumor cells decreased markedly after administration of rabdoternin E. Taken together, rabdoternin E induced apoptosis and ferroptosis of A549 cells by activating the ROS/p38 MAPK/JNK signaling pathway. Therefore, the results of the present study showed that rabdoternin E is not toxic to MCF-7 cells (normal lung cells), had no significant effect on body weight and was effective and therefore may be a novel therapeutic treatment for lung cancer.

Correspondence to: Professor Tao Guo, School of Pharmacy, Henan University of Chinese Medicine, 156 Jinshui East Road, Zhengzhou, Henan 450046, P.R. China
E-mail: gt010010@hactcm.edu.cn

*Contributed equally

Key words: rabdoternin E, A549 cells, apoptosis, ferroptosis, p38, MAPK/JNK signaling pathway

Introduction

Lung cancer is the leading cause of cancer-related deaths worldwide, accounting for 18% of all cancer deaths. According to survey data in 2020, the incidence of lung cancer was second only to breast cancer globally and both morbidity and mortality rates continue to rise (1,2). Lung cancer is categorized into two main types: Small cell lung cancer and non-small cell lung cancer (NSCLC). NSCLC is most prevalent in the patient population and ~85% of lung cancer patients have NSCLC (3). The A549 cell line is derived from a primary lung tumor and is one of the most commonly used in the study of human NSCLC cell lines. In the face of persistently high incidence and mortality rates, the medical treatment of lung cancer must progress and more effective treatment methods need to be developed (4). Traditional lung cancer treatment methods mainly include surgery and chemotherapy (5). Current therapeutic approaches and strategies for lung cancer treatment have made progress, such as nanodrug delivery systems, molecularly targeted therapeutic systems, photothermal therapeutic strategies and lung cancer immunotherapy. These approaches have provided new perspectives and insights into the treatment of lung cancer (6). Unlike traditional cytotoxic drugs, targeted anti-tumor drugs mainly target components of cell signaling pathways, such as cycle-regulating proteins, immune regulatory factors and important proteins or factors involved in angiogenesis, with relatively high specificity (7,8). Compared with chemotherapy, targeted therapy is safer and more controllable (9). For example, following the application of tyrosine kinase inhibitors (TKI) in EGFR-positive NSCLC, overall survival is significantly increased (10) and TKI inhibitors exhibit fewer side effects

compared with chemotherapy (11). The development of targeted anti-tumor drugs has become the key focus of anti-tumor drug research (12). Therefore, seeking active ingredients with improved efficacy and lower toxicity in natural drugs provides novel avenues of research for tumor treatment.

Rabdoternin E is an ent-kaurane diterpene monomer compound and is commonly found in plants of the *Isodon* genus of the Lamiaceae family. It is reported that kaurene-type diterpenoids have significant anti-tumor activities (13), however, studies on the pharmacological activity associated with rabdoternin E have not been reported in the current literature. Our previous preliminary study found that rabdoternin E effectively inhibits the proliferation of lung cancer A549 cells (14). Therefore, the present study further investigated the inhibitory effect and underlying mechanisms of rabdoternin E on the proliferation of A549 cells and provide basic data for the study of the anti-tumor activity of rabdoternin E.

Materials and methods

Preparation of drugs. Rabdoternin E with >98% purity was supplied by Henan Engineering Research Center of Medicinal and Edible Chinese Medicine (Zhengzhou, China). Rabdoternin E was initially dissolved in culture medium (DMEM; Beijing Solarbio Science & Technology Co., Ltd.) at a concentration of 500 μM *in vitro* experiments and was subsequently diluted to 5, 10 and 15 μM. Rabdoternin E was dissolved in saline and formulated as a solution for oral administration in *in vivo* experiments. The stock solution concentrations of rabdoternin E in saline for *in vivo* use were 0.034, 0.068 and 0.136 mg/ml and the dosage of rabdoternin E was 0.1 ml/10 g.

Cell culture. The lung cancer cell line A549 was cultured in Dulbecco's Modified Eagle's Medium (Beijing Solarbio Science & Technology Co., Ltd.) supplemented with 10% fetal bovine serum (Gibco; Thermo Fisher Scientific, Inc.) at 37˚C in a 5% CO_2 environment. A549 cells were cultured at a maximum of 10 passages to ensure the integrity of the cell line. A549 cells and MRC-5 cells were obtained from Professor Chen Suiqing at Henan University of Chinese Medicine (Zhengzhou, China).

Cell viability assay. The cytotoxicity of rabdoternin E on A549 cells was measured by a 3-(4,5-dimethylthiazol 2-yl)-2,5-diphenyltetrazolium bromide (MTT; Beijing Solarbio Science & Technology Co., Ltd.) assay. In brief, A549 cells ($1x10^4$ cells/well) were seeded into a 96-well culture plate overnight and treated with 5, 10 and 15 μM of rabdoternin E for 24, 48 and 72 h. The cells were incubated with MTT (5 mg/ml) for 4 h and after which 150 μl DMSO (Beijing Solarbio Science & Technology Co., Ltd.) was added to each well and the cells were gently shaken for 10 min to completely dissolve the purple crystals. Finally, the absorbance values of each well were measured at 492 nm using a microplate reader (Infinite F50; Tecan Group, Ltd.) (15). Cell viability was calculated as the percentage of viable cells in the A549-treated group vs. the untreated control.

Clonogenic assay. The cells were seeded into 6-well plates (800 cells/well) and cultured for 24 h. After which, the culture medium was replaced with medium containing different final concentrations (0, 5, 10 and 15 μM) of rabdoternin E and incubated (37˚C) for another 24 h. The medium containing the drug was then removed and replaced with complete culture medium for 10 days, with regular medium changes during the culture period. After the culture period, the cells were washed twice with PBS, fixed with 4% paraformaldehyde (Beijing Solarbio Science & Technology Co., Ltd.) for 15 min at room temperature and then stained with 1% crystal violet (Beijing Solarbio Science & Technology Co., Ltd.) for 5 min. Excess staining solution was removed by washing with PBS and colonies were counted to calculate the cloning efficiency. The cell population clones were between 0.3-1.0 mm in size and each clone contained >50 cells.

Cell cycle analysis. Cells ($3x10^5$ cells/well) were seeded into a 6-well culture plate overnight for attachment and treated with 0, 5 10 and 15 μM of rabdoternin E for 24 h, washed twice with cold PBS and fixed in 70% ethanol at -4˚C for 12 h. After washing the fixed cells with 1 ml PBS and centrifuging (5 min; 85 x g; -4˚C), the supernatant was removed and 100 μl RNase A solution was added to the cell pellet. The cells were resuspended and incubated at 37˚C for 30 min. After which, 400 μl propidium iodide (PI) staining solution was added and mixed thoroughly. The cells were incubated in the dark at 4˚C for 30 min, filtered through a 200-mesh cell strainer and finally analyzed by flow cytometry (BD Accuri C6 Plus; BD Biosciences) (16).

FITC annexin V/PI apoptosis assay. Cells ($3x10^5$ cells/well) were seeded onto a 6-well culture plate overnight for attachment and treated with rabdoternin E (0, 5, 10 and 15 μmol/l) for 24 h at 37˚C with 5% CO_2. Apoptosis assay was performed using the FITC Annexin V Apoptosis Detection Kit (Beijing Solarbio Science & Technology Co., Ltd.). The cells were washed once with PBS, trypsinized and resuspended in media. A total of $1x10^5$ cells were centrifuged (5 min; 85 x g; -4˚C) and the cell pellets were washed with PBS, resuspended in 100 μl 1X binding buffer and then incubated with 3 μl FITC Annexin V and 5 μl PI for 15 min in the dark. Finally, all samples were analyzed by flow cytometry analysis using a BD Accuri C6 Flow Cytometer (BD Biosciences) (17).

Reactive oxygen species (ROS) assay. Detection of intracellular ROS was performed using DCEH-DA as a fluorescent probe. Cells were seeded in 6-well plates at a density of $3x10^5$ cells/well and incubated at 37˚C for 24 h. After treatment with 0, 5, 10 and 15 μM of rabdoternin E for 24 h, all cells were collected, washed twice with PBS and resuspended in 1 ml 10 μM DCEH-DA solution (loaded with probe) for 20 min at 37˚C. Finally, the cells were resuspended in 500 μl PBS and analyzed using flow cytometry (BD Accuri C6 Plus; BD Biosciences).

Determination of malondialdehyde (MDA) and glutathione (GSH) levels. MDA content and GSH activity were determined using the relevant kits (MDA; cat. no. BC0025; Beijing Solarbio Science & Technology Co., Ltd.; GSH; cat. no. BC1175; Beijing Solarbio Science & Technology Co., Ltd.) according to the manufacturer's instructions. After A549 cells were administered and treated for 24 h, cells were collected and lyzed by repeatedly

placing the cells in liquid nitrogen for 3-4 times. The lysed cells were centrifuged (10 min; 8,497 x g; -4˚C) and the supernatant was collected. The MDA and GSH contents of the samples were then determined according to the instructions of the two kits.

Western blot analysis. Total proteins were extracted from cells and tumor tissue, respectively. (RIPA lysate; cat. no. G2002; Wuhan Servicebio Technology Co., Ltd.). Protein concentration was assessed using a BCA assay kit (cat. no. G2026; Wuhan Servicebio Technology Co., Ltd.). Sodium dodecyl sulfate polyacrylamide gel electrophoresis was applied to separate proteins and the proteins were transferred to polyvinylidene fluoride membranes. The mass of protein per lane was 20 μg and the percentage of gel was 5%. After which, the membranes were blocked with 5% skimmed milk for 1 h at 37˚C and incubated at 4˚C overnight with the following primary antibodies: Bax, SCL7A11, glutathione peroxidase 4 (GPX4), Bcl-2, Ki67, Cyclin A2, CDK2 and GAPDH (cat. nos. GB114122, 1:1,000; DF12509, 1:1,000; DF12509, 1:1,000; GB113375, 1:1,000; GB11030, 1:1,000; GB11030, 1:1,000; GB112129, 1:1,000; GB15002, 1:2,000; Wuhan Servicebio Technology Co., Ltd.). Finally, the membranes were incubated with a goat anti-rabbit/mouse IgG HRP-linked antibody (cat. nos. GB23301 and GB23303; 1:5,000; CST Biological Reagents Co., Ltd.) for 2 h at room temperature. All bands were visualized by chemiluminescence. AlphaEaseFC 4.0 (Alpha Innotech) and Adobe PhotoShop 2024 (Adobe Systems, Inc.) were used for densitometry (18).

Lewis lung carcinoma mouse model. A total of 30 male BALB/c nude mice (4-6 weeks old; 18-20 g) were purchased from Beijing Vital River Laboratory Animal Technology Co., Ltd. They were given free access to food and water and kept in an SPF environment. The temperature in the environment was 24±2˚C, the relative humidity was 60%, and 12-h light/dark cycle. All experimental procedures were accomplished complying with the guidelines for the Care and Use of Laboratory Animals of Henan University of Chinese Medicine and approved by The Animal Experiments and Experimental Animal Management Committee from The Henan University of Chinese Medicine (Zhengzhou, China; approval no. DWLL202207009). BALB/c mice were injected subcutaneously with a total of $2x10^6$ A549 cells in the left forelimb. At 4 days after A549 inoculation, the mice were randomly divided into five groups (n=6/per group) including: i) Model group; ii) positive group (3 mg/kg cisplatin); iii) low rabdoternin E group (0.34 mg/kg); iv) medium rabdoternin E group (0.68 mg/kg); and v) high rabdoternin E group (1.36 mg/kg). Drug intervention groups were administered cisplatin or rabdoternin E by gavage for 15 consecutive days and the model group received the saline equivalent. The mice were weighed and tumor volume was measured with calipers every 3 days to track tumor growth and calculated according to the following formula: 0.5x length x $width^2$. The mice were sacrificed under deep anesthesia and tumor tissue was excised. No drugs were used to sacrifice the mice in this study. At the end of the experiment, Mice were anesthetized with 40 mg/kg pentobarbital sodium solution by intraperitoneal injection, blood was collected under anesthesia through heart puncture and then the mice were sacrificed by cervical dislocation and the collected samples were subsequently preserved at -80˚C for future use.

Histological analysis. Mouse tumor tissues were dissected and removed, washed in saline, weighed and recorded, and then fixed in 4% paraformaldehyde for 24 h at room temperature. Residual fixative on the samples was rinsed with running water, and then the fixed tissues were dehydrated in a gradient with ethanol at concentrations of 70, 80, 90, 95 and 100% in turn, with each concentration of ethanol solution being immersed for 2 h at room temperature. After the tissues were dehydrated, the tissues were placed in xylene I solution and xylene II solution and xylene II solution, respectively, for 15 min at room temperature, in turn. After tissue dehydration, the tissues were sequentially immersed in xylene I solution (ethanol:xylene=1:1), xylene II solution (ethanol:xylene=1:2) and xylene solution for 15 min at room temperature. Then the tumor tissues were sequentially placed in solution I (paraffin:xylene=1:1) solution II (paraffin:xylene=2:1) and paraffin for 1.5 h at room temperature to complete the wax infiltration. The embedded paraffin tissue was cut into sections of 3 μm thickness, transferred to slides heated at 60˚C for 30 min and stored at room temperature. Sections were placed into a staining cylinder and stained with hematoxylin staining solution for 10 min at room temperature. The section was removed and washed until no further dye washed out. The cells were differentiated with 1% hydrochloric ethanol differentiation solution for 3 sec, followed by rinsing with water for 5 min. Then, the sections were stained with eosin for 5 min at room temperature, followed by immersion in water for 2 min. The sections were successively dehydrated with 85 and 95% ethanol for 2 min at room temperature. Finally, the slices were placed in anhydrous ethanol for 5 min and placed in xylene for 5 min at room temperature. After drying the xylene, neutral resin was added to the front side to seal the sections. The typical histopathological changes of the tissues were observed under a light microscope (Eclipse Ci; Nikon Corporation) following the staining with an H&E staining kit (Wuhan Servicebio Technology Co., Ltd., China).

Statistical analysis. All data were presented as the mean ± standard deviation. Student's t-test was used to compare the differences between two groups and one-way analysis of variance was used to analyze differences among three or more groups, followed by Tukey's post hoc analyses for between-group comparisons. Statistical analysis was performed using the SPSS 26.0 statistical package (IBM Corp.). $P<0.05$ was considered to indicate a statistically significant difference.

Results

Rabdoternin E significantly inhibited the proliferation of A549 cells in vitro. Rabdoternin E is an ent-kaurane diterpene monomer compound (Fig. 1A). The MTT method was used to detect the effects of rabdoternin E at different concentrations on the proliferation of A549 cells. The proliferation of A549 cells was significantly inhibited by rabdoternin E intervention (Fig. 1B). Rabdoternin E inhibited A549 cell proliferation jto a greater degree than cisplatin (positive control) during the 24-h period with the IC_{50} of rabdoternin E and cisplatin against A549 cells 16.45 and 39.52 μM, respectively (Fig. 1C). In order to verify whether rabdoternin E has cytotoxicity on normal lung cells at tested concentrations for 24 h, the human embryonic lung fibroblast cell

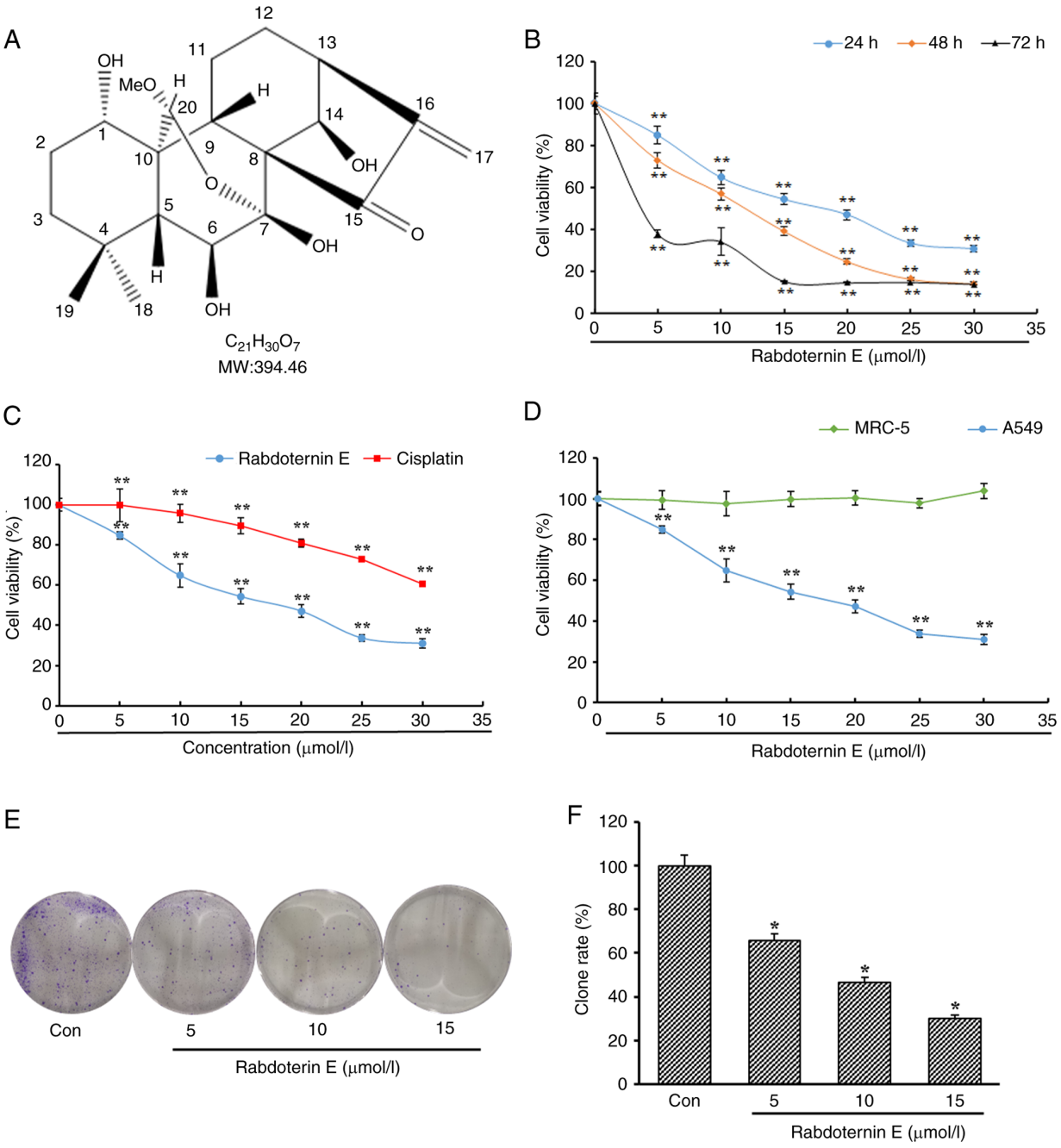


Figure 1. Proliferation inhibition of rabdoternin E on A549 cells *in vitro*. (A) Chemical structure of rabdoternin E. (B) Time-dependent cytotoxicity of rabdoternin E on A549 cells. (C) Effect of rabdoternin E and cisplatin treatment for 24 h on A549 cell viability. (D) Cytotoxicity of rabdoternin E on human embryonic lung fibroblast MRC-5 cells. (E) Effect of rabdoternin E on the clonogenic ability of A549 cells. (F) Effect of rabdoternin E on clonogenic ability of A549 cells ($\bar{x}\pm s$; n=6) $^{*}P<0.05$, $^{**}P<0.01$ vs. Con group. Con, control.

line MRC-5 was selected for cytotoxicity tests. The rabdoternin E had no toxic effect on MRC-5 cells at the tested concentrations (Fig. 1D). To further examine the inhibition of rabdoternin E on the proliferation of A549 cells, a clone formation assay was used to investigate the results. The number of cell clones significantly declined in a dose-dependent manner (Fig. 1E and F), which macroscopically confirms that rabdoternin E can significantly inhibit the proliferation of A549 cells.

Rabdoternin E can promote S phase arrest and induce apoptosis in A549 cells. Cell cycle progression is closely related to cell proliferation and complete and orderly cycle progression is the key to cell growth and proliferation (19,20). Compared with the control (Con) group, the proportion of cells in the S-phase in the rabdoternin E group significantly increased in a dose-dependent manner (Fig. 2A and C). When the dose of rabdoternin E reached 15 μM, the proportion of cells in the S phase reached 52.2%. The apoptosis rates in the Con group and rabdoternin E group at concentrations of 5, 10 and 15 μM for 24 h were 6.00, 8.19, 22.51 and 33.25%, respectively (Fig. 2B and D). The apoptosis rate in all tested groups was higher than that in the Con group ($P<0.05$ or $P<0.01$). As shown in Fig. 2E-I, Bax and Bcl-2 were dose-dependently up- and downregulated, respectively and the Bax/Bcl-2

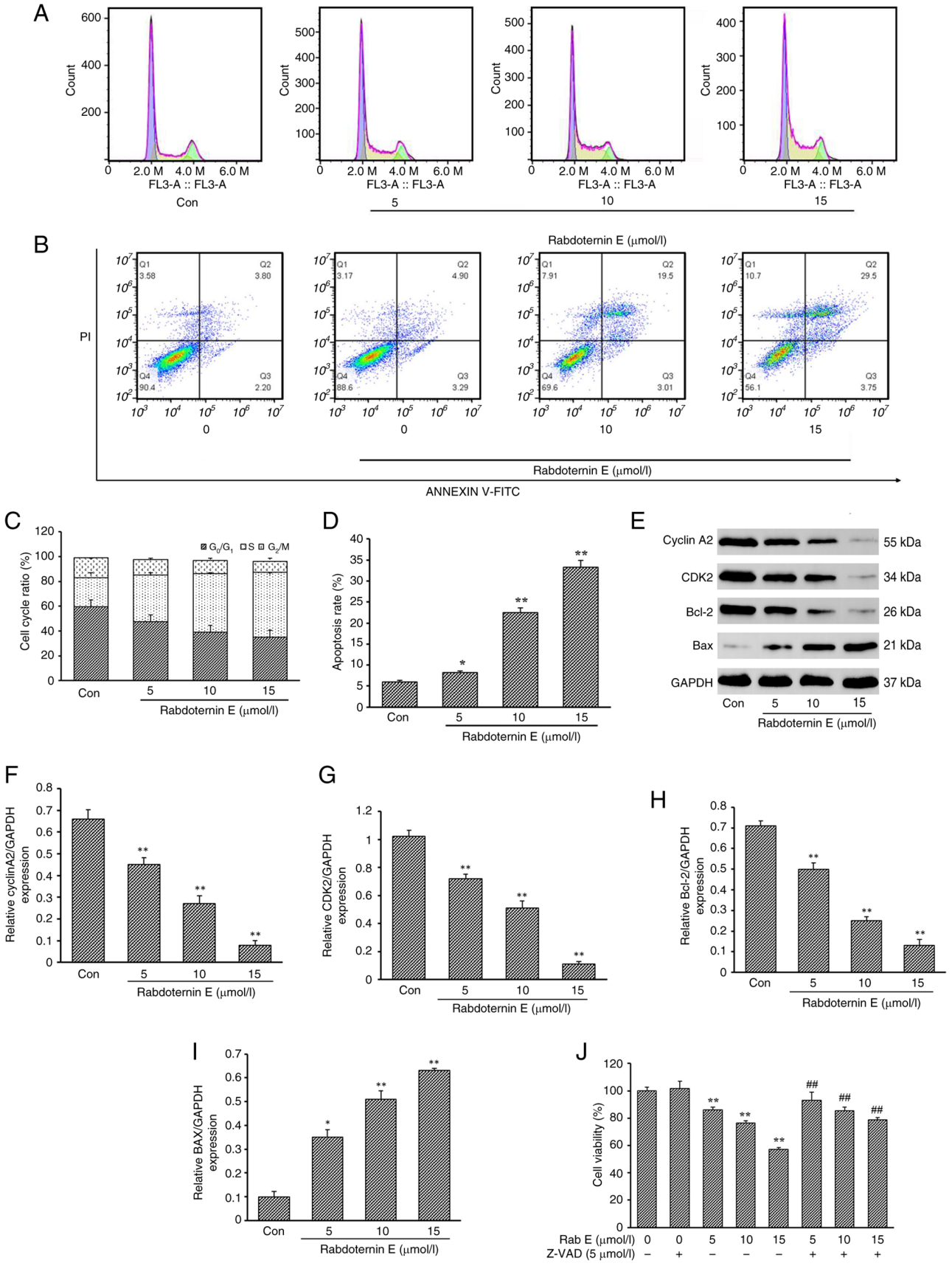


Figure 2. Rabdoternin E arrests the cell cycle in the S phase and induces apoptosis. (A) Effect of rabdoternin E on the cell cycle of A549 cells. (B) Effect of rabdoternin E on apoptosis of A549 cells. (C) With a rising concentration of rabdoternin E, the percentage of cells in S phase increased. (D) With increasing rabdoternin E concentration, the proportion of apoptotic cells gradually increased. (E) Effect of rabdoternin E on the expression of Cyclin A2, CDK2, Bcl-2 and Bax proteins in A549 cells. (F) Protein Cyclin A2 was dose-dependently downregulated (G) Protein CDK2 is dose-dependently downregulated. (H) The anti-apoptotic protein Bcl-2 was dose-dependently downregulated. (I) Pro-apoptotic protein Bax was dose-dependently upregulated. (J) Effect of co-culture using rabdoternin E and Z-VAD-FMK on cell viability. ($\bar{x}\pm s$; n=6) *P<0.05, **P<0.01, vs. Con group; $^{\#\#}$P<0.01, vs. apoptosis inhibitor only group. PI, propidium iodide; Con, control.

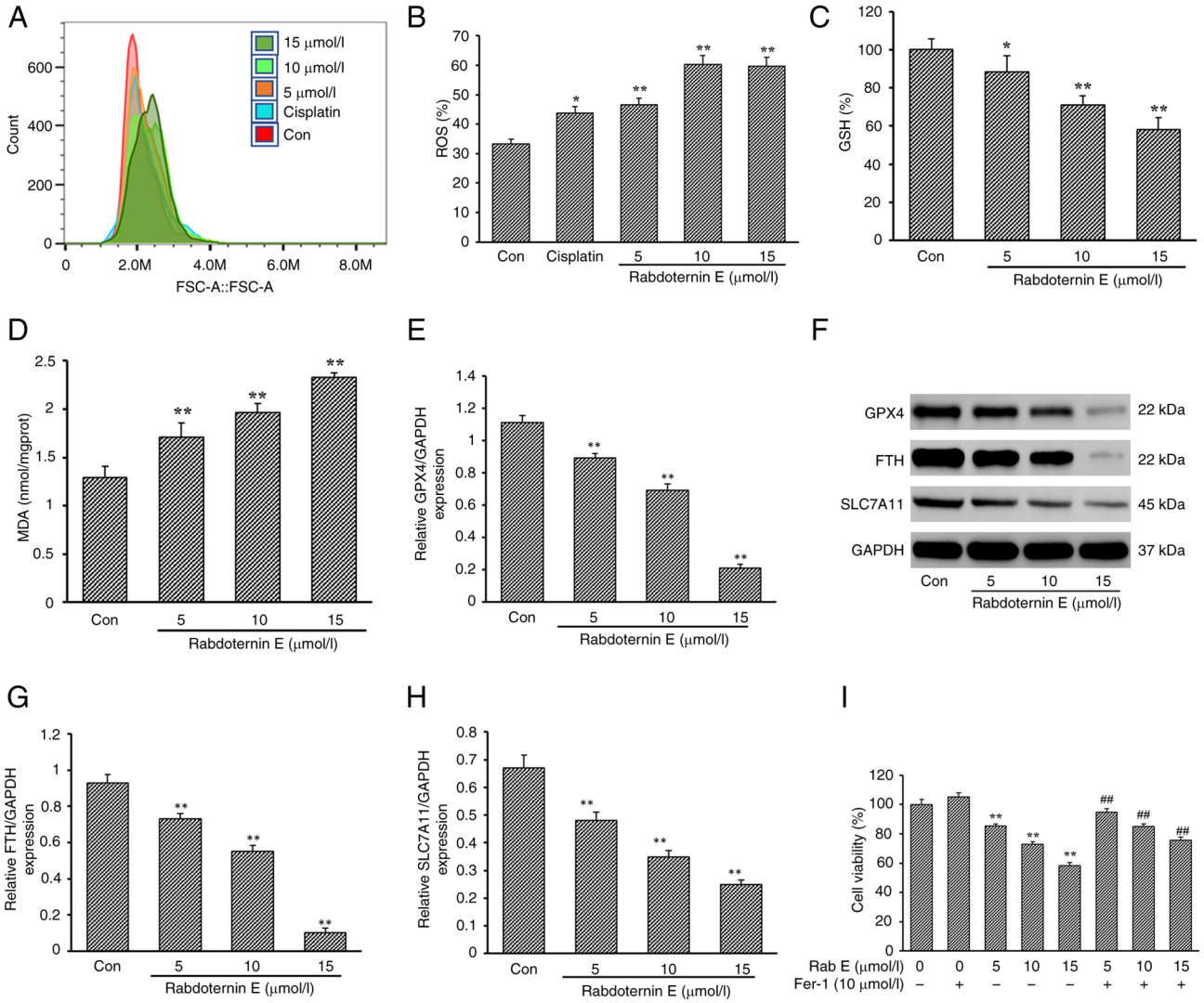


Figure 3. Effect of Rab E on ferroptosis of A549 cells. (A) Effects of different concentrations (5, 10 and 15 μM) of Rab E on intracellular ROS levels in A549 cells and (B) quantitative analysis. Effect of Rab E treatment for 24 h on the expression of (C) GSH and (D) MDA as indicators associated with ferroptosis. (E) Protein expression of GPX4, FTH and SLC7A11 in A549 cells treated with Rab E. (F-H) Effect of Rab E on the protein expression of (F) GPX4, (G) FTH and (H) SLC7A11 in A549 cells. (I) Co-culture using ferroptosis-inhibiting Fer-1 and Rab E significantly reversed cell viability in A549 cells. ($\bar{x}\pm s$; n=6) *P<0.05, **P<0.01, vs. Con group; $^{\#\#}$P<0.01, vs. Fer-1 group with ferroptosis inhibitor only. ROS, reactive oxygen species; GSH, glutathione; MDA, malondialdehyde; GPX4, glutathione peroxidase; FTH, ferritin heavy; SLC7A11, solute carrier family 7 member 11; Rab E, rabdoternin E; Fer-1, ferrostatin-1; Con, control.

ratio increased. Moreover, the expression of S-phase related proteins CDK2 and Cyclin A2 decreased significantly with the increase of the rabdoternin E concentration. Finally, rabdoternin E and the apoptosis inhibitor Z-VAD-FMK (10 μM) were co-cultured for 24 h. Z-VAD-FMK reversed the cytotoxicity of rabdoternin E on A549 cells by ~10% (P<0.05 or P<0.01), indicating that rabdoternin E induces apoptosis in A549 cells (Fig. 2J). However, apoptosis is not the only cause of drug-induced cell death and the effects of rabdoternin E may be caused by other forms of cell death (21,22).

Rabdoternin E induces ferroptosis in A549 cells. In the process of cancer treatment, drug stimulation can increase the level of ROS expression, which in turn induces apoptosis and serves to inhibit the proliferation and spread of cancer cells (23,24). Meanwhile, the accumulation of ROS can induce the occurrence of intracellular ferroptosis (25,26). In the present study, the level of ROS following rabdoternin E treatment significantly increased in a dose-dependent manner (Fig. 3A and B). A previous studies showed that ROS accumulation disrupts GSH/GSSH homeostasis, causing GSH depletion, inducing lipid peroxidation and leading to the occurrence of ferroptosis (27,28). Combined with the fact that the apoptosis inhibitor Z-VAD-FMK and rabdoternin E co-culture did not completely reverse the proliferation inhibitory effect of rabdoternin E on A549 cells, changes in GSH and MDA (indicators associated with ferroptosis) levels after 24 h of rabdoternin E treatment were examined. Rabdoternin E caused intracellular GSH depletion and MDA accumulation in a dose-dependent manner (P<0.05 or P<0.01, respectively; Fig. 3C and D), indicating the occurrence of ferroptosis in cells.

Compared with the Con group, the expression of ferroptosis marker proteins including solute carrier family 7 member 11 (SLC7A11), GPX4 and ferritin heavy (FTH) decreased in a dose-dependent manner after rabdoternin E treatment for 24 h (Fig. 3E-H). Furthermore, the co-culture of rabdoternin E

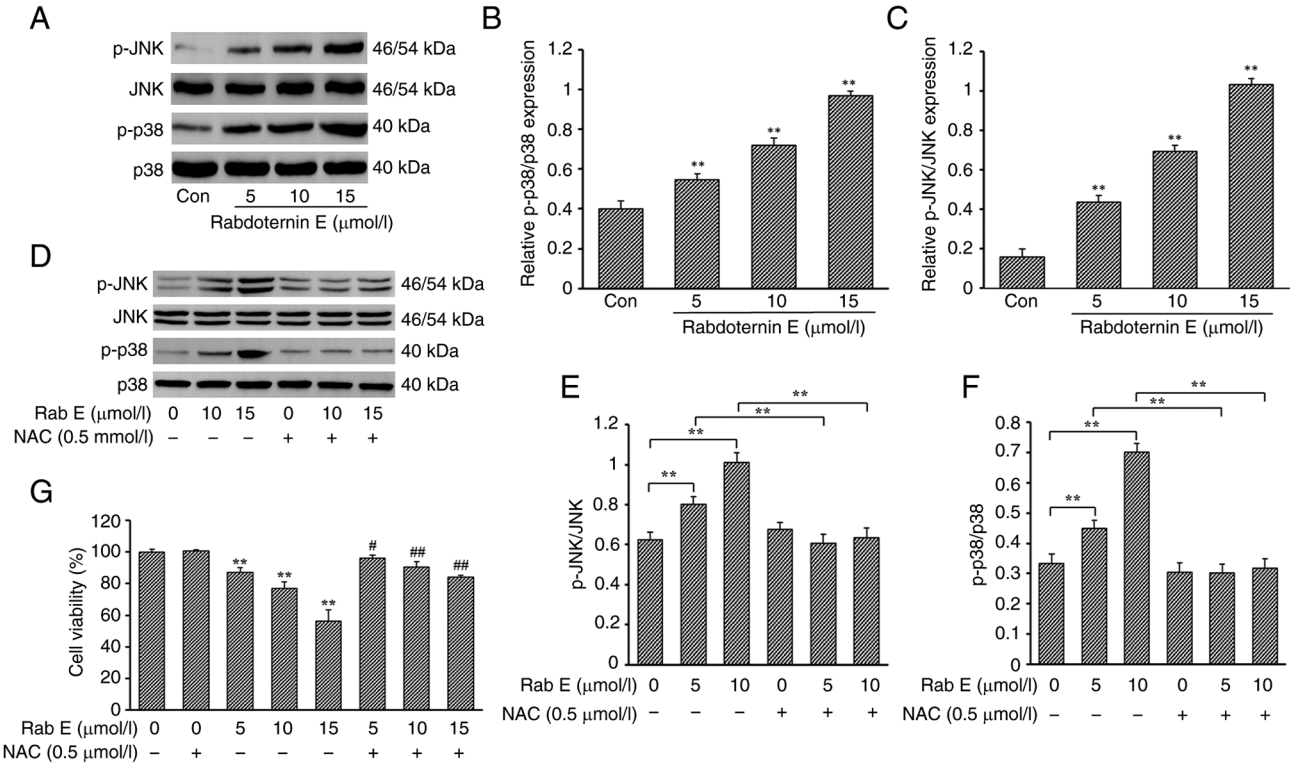


Figure 4. Effect of Rab E on ROS-dependent p38 MAPK/JNK Pathway. (A) Effect of Rab E on p-p38 MAPK and JNK protein expression in A549 cells. Effect of different concentrations (5, 10 and 15 μmol/l) of Rab E on (B) p38 MAPK and (C) JNK protein expression in A549 cells. (D) Expression levels of p38 MAPK and JNK after co-cultured treatment with the ROS inhibitor NAC and different concentrations of Rab E. (E and F) Effect of co-culture of rabdoternin E and inhibitor NAC on (E) JNK and (F) p38 MAPK protein expression in A549 cells. (G) Survival of A549 cells after 24 h of co-culture of NAC and Rab E. ($\bar{x}\pm s$; n=6) **P<0.01, vs. Con group; $^{\#}$P<0.05, $^{\#\#}$P<0.01, vs. the group with only the ROS inhibitor NAC. Rab E, rabdoternin E; ROS, reactive oxygen species; NAC, N-acetylcysteine; p-, phosphorylated; Con, control.

and a ferroptosis inhibitor ferrostatin-1 significantly reversed the inhibitory effect of rabdoternin E on A549 cells, suggesting that rabdoternin E induced ferroptosis in A549 cells (Fig. 3I).

Effect of rabdoternin E on the ROS-dependent p38 MAPK/JNK pathway. To verify whether rabdoternin E regulates apoptosis and ferroptosis in A549 cells through the p38 MAPK/JNK pathway, the expression of phosphorylated p38 MAPK and JNK in A549 cells following rabdoternin E treatment was examined. The phosphorylation levels of p38 MAPK and JNK increased in a dose-dependent manner, indicating that rabdoternin E could effectively regulate the transactivation of the p38 MAPK/JNK signaling pathway in A549 cells (Fig. 4A-C). The phosphorylation levels of p38 MAPK and JNK in cells by co-cultured experiments with the ROS inhibitor N-acetylcysteine (NAC) and rabdoternin E were examined. NAC treatment effectively inhibited rabdoternin E-stimulated p38 MAPK and JNK activation (P<0.05 or P<0.01; Fig. 4D-F). The addition of NAC effectively reversed the cytotoxicity of rabdoternin E on A549 and the degree of reversal was significantly stronger than the effects of the apoptosis inhibitor or ferroptosis inhibitor (Fig. 4G). Therefore, the results indicated that the ROS-dependent activation of the p38 MAPK/JNK pathway is associated with rabdoternin E-induced apoptosis and ferroptosis in A549 cells.

Rabdoternin E inhibits tumor growth and induces tumor cell death in vivo. To verify the anti-tumor effect of rabdoternin E *in vivo* using a Lewis lung carcinoma mouse model, BALB/c mice were treated with rabdoternin E for 21 days (Fig. 5). The tumor volume and mass in the rabdoternin E group at all doses was significantly reduced compared with the model group of BALB/c nude mice and those of the high and middle dosage rabdoternin E group were smaller compared with the cisplatin group (Fig. 6A, B and D). Moreover, all tested doses of rabdoternin E did not significantly affect the body weight of BALB/c nude mice, indicating that rabdoternin E had no significant toxic side effects in the mice, but the positive dose group showed the greatest change in body weight, with a 14.82% decrease in body weight from the beginning of the experiment to the end of the experiment (Fig. 6C). H&E staining showed that the tumor cells were regularly, neatly and tightly packed in the model group, while those in the rabdoternin E groups were disorganized with large cell gaps, severely vacuolated and the number significantly reduced, suggesting rabdoternin E significantly inhibited the proliferation of A549 cell (Fig. 6E). rabdoternin E treatment significantly decreased the expressions of Bcl-2, Ki67, GPX4 and SLC7A11 (P<0.01) and increased those of Bax and transferrin in the tumor tissues (Fig. 6F-L), indicating that rabdoternin E induces apoptosis and iron death via ROS-dependent p38 MAPK/JNK pathway activation.

Discussion

At present, there are no literature reports on the mechanisms of anti-tumor action of rabdoternin E. In the present study, it was found that rabdoternin E induced apoptosis and ferroptosis

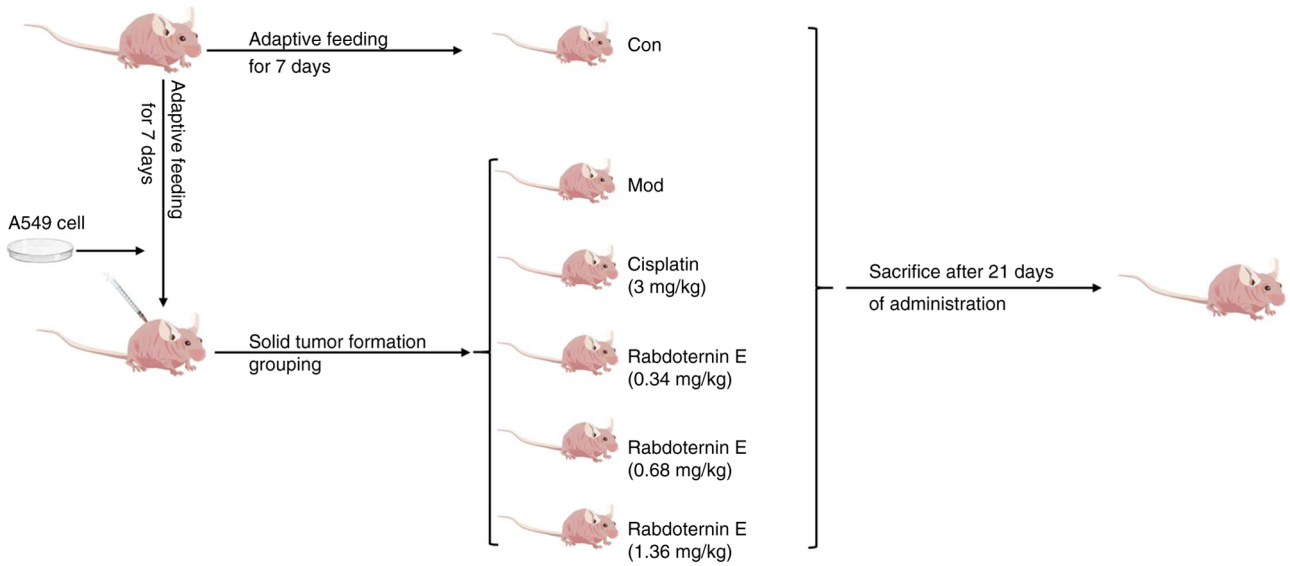


Figure 5. Schematic diagram of the animal experiment. Con, control; Mod, model group.

in A549 cells through the ROS/p38MAPK/JNK signaling pathway. The MTT experiments demonstrated that rabdoternin E significantly inhibited the proliferation of A549 cells with an IC_{50} value of 16.4 μM and was not cytotoxic to normal lung cells (MRC-5). Numerous ent-Kaurane diterpenoids have been reported to have marked anti-lung cancer activity (14). For example, rabdoternin F and Isorosthin O significantly inhibit A549 cell proliferation with IC_{50} values of 18.1 and 18.8 μM, respectively, thus indicating that rabdoternin E has greater inhibitory activity against A549 cells. However, numerous ent-kaurane diterpenoids including rabdoternin E, rabdoternin F and Isorosthin O have weak inhibitory activity against the proliferation of SMMC7721 and SW480 cells (14).

In order to explore the mechanisms behind this action, apoptosis and cell cycle-related analyses were conducted on rabdoternin E-treated cells. The findings of the present study revealed that rabdoternin E arrests the cell cycle in the S phase and induces apoptosis. In addition, it was noted that ROS levels increased in rabdoternin E-treated cells. It is well established that ROS accumulation is often associated with disturbances in cellular oxidative disorders (29,30). Subsequent co-culture studies with rabdoternin E and Z-VAD-FMK (an apoptosis inhibitor) showed a partial reversal of the cytotoxicity of rabdoternin E to A549 cells. Therefore, it was hypothesized that in addition to inducing apoptosis, rabdoternin E may contribute to cell death through oxidative metabolic disorders. The occurrence of ferroptosis primarily arises from intracellular GSH depletion and reduced activity of GPX4, resulting in impaired metabolism of lipid peroxides through GPX4-catalyzed reduction reactions (31,32). Simultaneously, the Fenton reaction oxidizes lipids and generates a substantial amount of ROS, thereby accelerating cell death (33). Previous studies have demonstrated that ferroptosis is strongly linked with the regulation and pathophysiological processes underlying tumors, nervous system disorders, kidney injury and hematologic diseases (34-37).

Rabdoternin E significantly decreased the GSH content and increased the MDA content in cells. Moreover, ferrostatin-1 (a ferroptosis inhibitor) effectively reduced the inhibitory effect of rabdoternin E on A549 cells. These findings strongly suggested that rabdoternin E induced ferroptosis. Additionally, it was found that rabdoternin E markedly downregulated the expression of SLC7A11 and GPX4 in cells, indicating it regulated ferroptosis through modulating the SLC7A11/GPX4 axis. SLC7A11, as an important regulator of ferroptosis sequestration, plays a crucial role in various regulatory processes such as tumorigenesis, proliferation, metastasis, prognosis and chemotherapy resistance (38,39).

Studies have demonstrated that ROS possess the ability to facilitate signaling pathways in tumor cells and induce oxidative stress, ultimately leading to cellular apoptosis. Consequently, ROS has emerged as a promising target for potential cancer therapies (40,41). The MAPK signal transduction pathway plays a crucial role in various physiological processes and oxidative stress (42) and the activation of MAPK regulates cell proliferation, apoptosis, invasion and metastasis in numerous tumor cells (43,44). Among the MAPK signaling pathways, p38 MAPK and JNK are important downstream effectors of ROS (45,46). Excessive ROS can activate the downstream p38 MAPK/JNK pathway, leading to increased expression levels of proapoptotic proteins and induction of apoptosis (47). Additionally, the MAPK signaling pathways are involved in regulating ferroptosis (48).

The object of the present study was to investigate the regulatory effects of rabdoternin E on apoptosis and ferroptosis in A549 cells through the ROS-mediated p38 MAPK/JNK pathway (Fig. 7). It was also found that the phosphorylation levels of p38 MAPK and JNK increased dose-dependently following rabdoternin E treatment. Notably, co-treatment experiments with NAC and rabdoternin E demonstrated that the phosphorylation levels of p38 MAPK and JNK in A549 cells and the cytotoxicity induced by rabdoternin E were markedly reduced. The present study indicated that rabdoternin E induces intracellular accumulation of ROS, which not only activates downstream effectors such as p38 MAPK and JNK

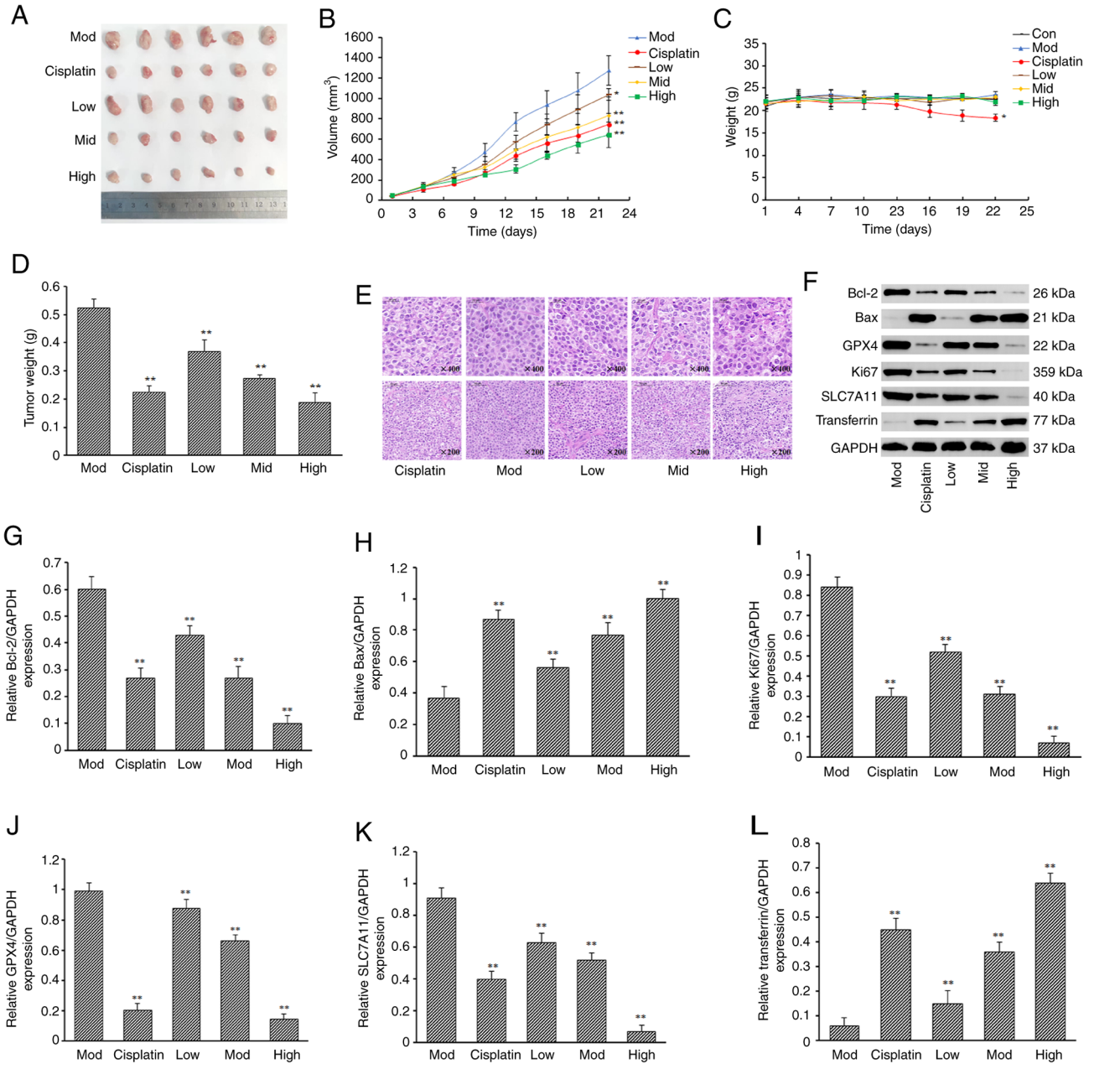


Figure 6. Effect of rabdoternin E on the proliferation of subcutaneous transplanted tumors in nude mice with human lung cancer A549 cells. Plots of (A) tumor appearance, (B) tumor size and (C) body weight of mice in each group. (D) Tumor weight. (E) H&E staining results of tumor tissues in each group. Magnification, x200 and x400. (F) Protein bands of each experimental group. Protein expression of (G) Bcl-2, (H) Bax, (I) Ki67, (J) GPX4, (K) SLC7A11 and (L) transferrin of each experimental group. ($\bar{x}\pm s$; n=6) *P<0.05, **P<0.01, vs. Mod group. GPX4, glutathione peroxidase; SLC7A11, solute carrier family 7 member 11; Mod, model group.

that promote apoptosis and ferroptosis, but also leads to lipid peroxide accumulation in cells, further inducing iron-dependent cell death.

In the *in vivo* animal experiments, a potent inhibitory effect of rabdoternin E on tumor growth activity was observed. Compared with the control group, rabdoternin E significantly slowed down the growth rate of tumors in mice, resulting in smaller tumor volume and mass. Notably, the mice in the administered group at the medium and high doses of rabdoternin E had a smaller tumor volume and mass than the cisplatin group, indicating that rabdoternin E also has strong tumor growth inhibitory activity *in vivo*. Moreover, the body weight of mice in the rabdoternin E groups were not adversely affected. However, over the course of the present study, the body weight of the mice in the cisplatin group significantly decreased. Western blotting results showed that the expression content of Ki67 protein decreased with the increase of administered dose and the weakening of Ki67 protein expression implied the decrease of tumor proliferation ability. At the same time, it was found that the apoptosis-related Bax/Bcl-2 protein expression ratio increased. Ultimately, they together promote apoptosis of tumor cells.

Meanwhile, western blotting of tumor tissues revealed that the expression levels of SLC7A11 and GPX4 were significantly reduced in tissues after rabdoternin E administration compared to controls. Therefore, it was concluded that rabdoternin E-induced downregulation of SLC7A11 and GPX4 plays a critical role in regulating ferroptosis in A549 cells.

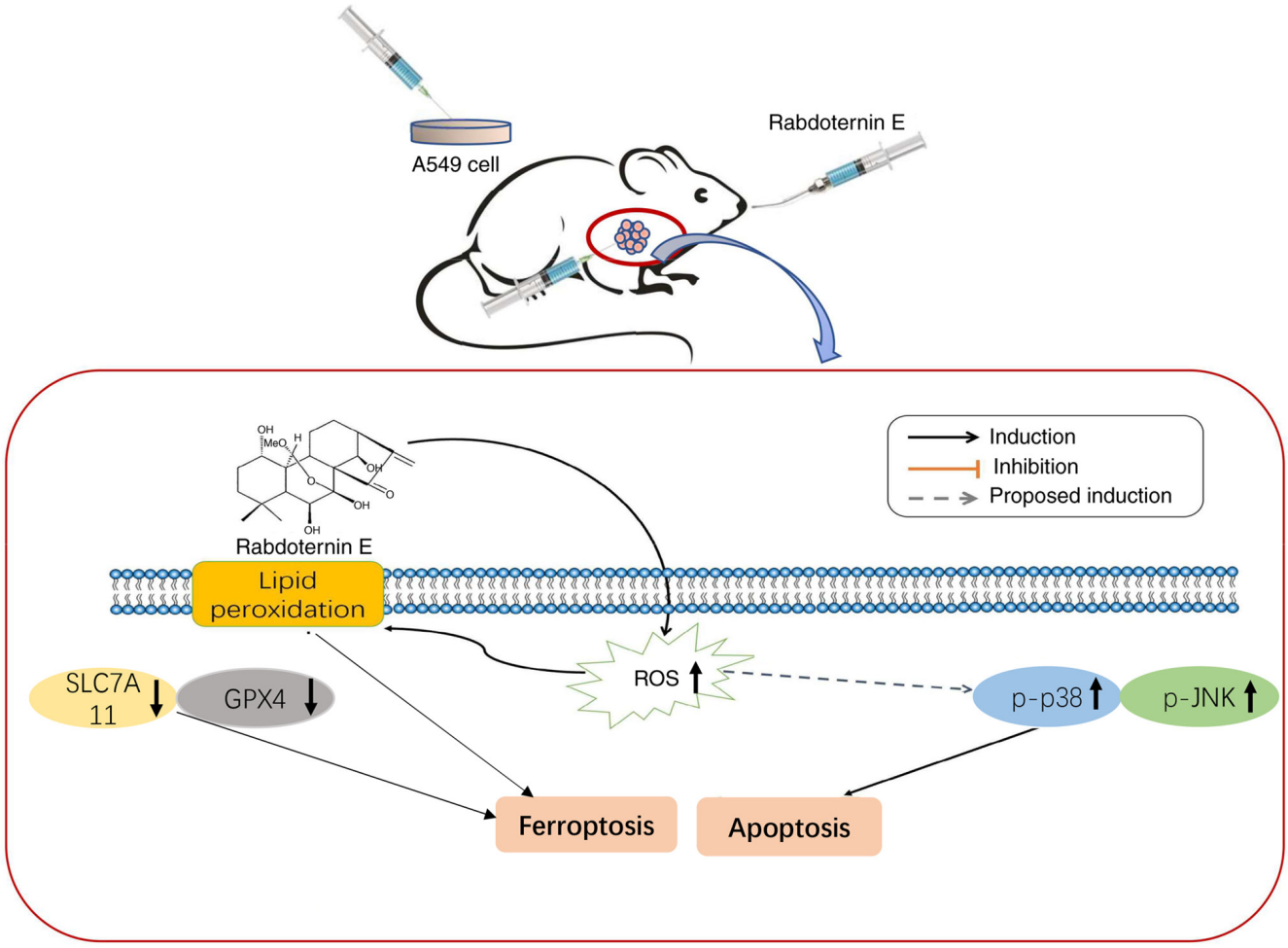


Figure 7. Mechanism of rabdoternin E inhibiting proliferation of A549 cells. p-, phosphorylated; GPX4, glutathione peroxidase; SLC7A11, solute carrier family 7 member 11.

To conclude, in the present study rabdoternin E effectively inhibited A549 cell proliferation *in vitro* through induction of the apoptosis and ferroptosis pathways.

Acknowledgements

Not applicable.

Funding

The present study was funded by the High-Level Talents International Training project of Henan Province (grant no. 2021-72) and Major Science and Technology Programs in Henan Province (grant no. 221100310400).

Availability of data and materials

The data generated in the present study may be requested from the corresponding author.

Authors' contributions

JJ, JN and TG designed the experiments. JJ, JN and YS performed most of the data analysis and animal and cell experiments. XC, HW, XW and JH collected and analyzed the data. JJ and JN wrote the manuscript. YS revised the manuscript. TG and YS confirm the authenticity of all the raw data. All authors read and approved the final manuscript.

Ethics approval and consent to participate

All experiments on animals were approved by the Subcommittee on Henan University of Traditional Chinese Medicine Animal Experiment Center (approval no. DWLL202207009).

Patient consent for publication

Not applicable.

Competing interests

The authors declare that they have no competing interests.

References

1. Li C, Lei S, Ding L, Xu Y, Wu X, Wang H, Zhang Z, Gao T, Zhang Y and Li L: Global burden and trends of lung cancer incidence and mortality. Chin Med J (Engl) 136: 1583-1590, 2023.

2. Huang J, Deng Y, TinM S, Lok V, Ngai CH, Zhang L, Lucero-Prisno DE III, Xu W, Zheng ZJ, Elcarte E, *et al*: Distribution, risk factors, and temporal trends for lung cancer incidence and mortality: A global analysis. Chest 161: 1101-1111, 2022.
3. Tandberg DJ, Tong BC, Ackerson BG and Kelsey CR: Surgery versus stereotactic body radiation therapy for stage I non-small cell lung cancer: A comprehensive review. Cancer 124: 667-678, 2018.
4. LeeC S, Shu CC, Chen YC, Liao KM and Ho CH: Tuberculosis treatment incompletion in patients with lung cancer: Occurrence and predictors. Int J Infect Dis 113: 200-206, 2021.
5. Tartour E and Zitvogel L: Lung cancer: Potential targets for immunotherapy. Lancet Respir Med 1: 551-563, 2013.
6. LiY, Yan B and He S: Advances and challenges in the treatment of lung cancer. Biomed Pharmacother 169: 115891, 2023.
7. Liu S, Bishop WR and Liu M: Differential effects of cell cycle regulatory protein p21(WAF1/Cip1) on apoptosis and sensitivity to cancer chemotherapy. Drug Resist Updat 6: 183-195, 2003.
8. Chin EN, Sulpizio A and Lairson LL: Targeting STING to promote antitumor immunity. Trends Cell Biol 33: 189-203, 2023.
9. Pérez-Herrero E and Fernández-Medarde A: Advanced targeted therapies in cancer: Drug nanocarriers, the future of chemotherapy. Eur J Pharm Biopharm 93: 52-79, 2015.
10. Jurisic V, Vukovic V, Obradovic J, Gulyaeva LF, Kushlinskii NE and Djordjević N: EGFR polymorphism and survival of NSCLC patients treated with TKIs: A systematic review and meta-analysis. J Oncol 2020: 1973241, 2020.
11. Obradovic J, Todosijevic J and Jurisic V: Side effects of tyrosine kinase inhibitors therapy in patients with non-small cell lung cancer and associations with EGFR polymorphisms: A systematic review and meta-analysis. Oncol Lett 25: 62, 2022.
12. Nishimoto A: Effective combinations of anti-cancer and targeted drugs for pancreatic cancer treatment. World J Gastroenterol 28: 3637-3643, 2022.
13. Fujita E, Nagao Y, Kaneko K, Nakazawa S and Kuroda H: The antitumor and antibacterial activity of the Isodon diterpenoids. Chem Pharm Bull (Tokyo) 24: 2118-2127, 1976.
14. Wei WJ, Zhu B, Si Y, Guo T, Kang J and Dai L: Cytotoxic ent-kaurane diterpenoids from rabdosia rubescens. Chem Biodivers 19: e202200497, 2022.
15. Jia XB, Zhang Q, Xu L, Yao WJ and Wei L: Lotus leaf flavonoids induce apoptosis of human lung cancer A549 cells through the ROS/p38 MAPK pathway. Biol Res 54: 7, 2021.
16. Jin X, Sun PP, Hong Y, Yu L and Li S: Puerarin induces apoptosis in A549 cells. Zhongguo Ying Yong Sheng Li Xue Za Zhi 33: 466-469, 2017 (In Chinese).
17. Zhao C, Qin G, Gao W, Chen J, Liu H, Xi G, Li T, Wu S and Chen T: Potent proapoptotic actions of dihydroartemisinin in gemcitabine-resistant A549 cells. Cell Signal 26: 2223-2233, 2014.
18. Zhou T, Qin R, Shi S, Zhang H, Niu C, Ju G and Miao S: DTYMK promote hepatocellular carcinoma proliferation by regulating cell cycle. Cell Cycle 20: 1681-1691, 2021.
19. Oredsson SM: Polyamine dependence of normal cell-cycle progression. Biochem Soc Trans 31: 366-370, 2003.
20. Guarracino MR, Xanthopoulos P, Pyrgiotakis G, Tomaino V, Moudgil BM and Pardalos PM: Classification of cancer cell death with spectral dimensionality reduction and generalized eigenvalues. Artif Intell Med 53: 119-125, 2011.
21. Efimova I, Catanzaro E, Van der Meeren L, Turubanova VD, Hammad H, Mishchenko TA, Vedunova MV, Fimognari C, Bachert C, Coppieters F, *et al*: Vaccination with early ferroptotic cancer cells induces efficient antitumor immunity. J Immunother Cancer 8: e001369, 2020.
22. Martinvalet D: ROS signaling during granzyme B-mediated apoptosis. Mol Cell Oncol 2: e992639, 2015.
23. Al-Khayal K, Alafeefy A, Vaali-Mohammed MA, Mahmood A, Zubaidi A, Al-Obeed O, Khan Z, Abdulla M and Ahmad R: Novel derivative of aminobenzenesulfonamide (3c) induces apoptosis in colorectal cancer cells through ROS generation and inhibits cell migration. BMC Cancer 17: 4, 2017.
24. Li Z, Xiao J, Liu M, Cui J, Lian B, Sun Y and Li C: Notch3 regulates ferroptosis via ROS-induced lipid peroxidation in NSCLC cells. FEBS Open Bio 12: 1197-1205, 2022.
25. Wang CX, Chen LH, Zhuang HB, Shi ZS, Chen ZC, PanJ P and Hong ZS: Auriculasin enhances ROS generation to regulate colorectal cancer cell apoptosis, ferroptosis, oxeiptosis, invasion and colony formation. Biochem Biophys Res Commun 587: 99-106, 2022.
26. Son Y, Kim S, Chung HT and Pae HO: Reactive oxygen species in the activation of MAP kinases. Methods Enzymol 528: 27-48, 2013.
27. Rochette L, Dogon G, Rigal E, Zeller M, Cottin Y and Vergely C: Lipid peroxidation and iron metabolism: Two corner stones in the homeostasis control of ferroptosis. Int J Mol Sci 24: 449, 2022.
28. Molavinia S, Dayer D, Khodayar MJ, Goudarzi G and Salehcheh M: Suspended particulate matter promotes epithelial-to-mesenchymal transition in alveolar epithelial cells via TGF-β1-mediated ROS/IL-8/SMAD3 axis. J Environ Sci (China) 141: 139-150, 2024.
29. Liu T, Sun L, Zhang Y, Wang Y and Zheng J: Imbalanced GSH/ROS and sequential cell death. J Biochem Mol Toxicol 36: e22942, 2022.
30. LiF J, Long HZ, Zhou ZW, Luo HY, Xu SG and Gao LC: System Xc^-/GSH/GPX4 axis: An important antioxidant system for the ferroptosis in drug-resistant solid tumor therapy. Front Pharmacol 13: 910292, 2022.
31. Xu Y, Li Y, Li J and Chen W: Ethyl carbamate triggers ferroptosis in liver through inhibiting GSH synthesis and suppressing Nrf2 activation. Redox Biol 53: 102349, 2022.
32. Miao Y, Chen Y, Xue F, Liu K, Zhu B, Gao J, Yin J, Zhang C and Li G: Contribution of ferroptosis and GPX4's dual functions to osteoarthritis progression. EBioMedicine 76: 103847, 2022.
33. Ma P, Xiao H, Yu C, Liu J, Cheng Z, Song H, Zhang X, Li C, Wang J, Gu Z and Lin J: Enhanced cisplatin chemotherapy by iron oxide nanocarrier-mediated generation of highly toxic reactive oxygen species. Nano Lett 17: 928-937, 2017.
34. Nie J, Lin B, Zhou M, Wu L and Zheng T: Role of ferroptosis in hepatocellular carcinoma. J Cancer Res Clin Oncol 144: 2329-2337, 2018.
35. Jia B, Li J, Song Y and Luo C: ACSL4-mediated ferroptosis and its potential role in central nervous system diseases and injuries. Int J Mol Sci 24: 10021, 2023.
36. Hou L, Li X, Su C, Chen K and Qu M: Current status and prospects of research on ischemia-reperfusion injury and ferroptosis. Front Oncol 12: 920707, 2022.
37. Li X, Zou Y, Fu YY, Xing J, Wang KY, Wan PZ and Zhai XY: A-lipoic acid alleviates folic acid-induced renal damage through inhibition of ferroptosis. Front Physiol 12: 680544, 2021.
38. Li S, Lu Z, Sun R, Guo S, Gao F, Cao B and Aa J: The role of SLC7A11 in cancer: Friend or foe? Cancers (Basel) 14: 3059, 2022.
39. Cheng X, Wang Y, Liu L, Lv C, Liu C and Xu J: SLC7A11, a potential therapeutic target through induced ferroptosis in colon adenocarcinoma. Front Mol Biosci 9: 889688, 2022.
40. Moloney JN and Cotter TG: ROS signalling in the biology of cancer. Semin Cell Dev Biol 80: 50-64, 2018.
41. Gerami P, Kim D, Compres EV, Zhang B, Khan AU, Sunshine JC, Quan VL and Busam K: Clinical, morphologic, and genomic findings in ROS1 fusion Spitz neoplasms. Mod Pathol 34: 348-357, 2021.
42. Lv C, Fu S, Dong Q, Yu Z, Zhang G, Kong C, Fu C and Zeng Y: PAGE4 promotes prostate cancer cells survive under oxidative stress through modulating MAPK/JNK/ERK pathway. J Exp Clin Cancer Res 38: 24, 2019.
43. Guimarães LM, Coura BP, Gomez RS and Gomes CC: The molecular pathology of odontogenic tumors: Expanding the spectrum of MAPK pathway driven tumors. Front Oral Health 2: 740788, 2021.
44. Li H, Han G, Li X, Li B, Wu B, Jin H, Wu L and Wang W: MAPK-RAP1A signaling enriched in hepatocellular carcinoma is associated with favorable tumor-infiltrating immune cells and clinical prognosis. Front Oncol 11: 649980, 2021.
45. Pereira L, Igea A, Canovas B, Dolado I and Nebreda AR: Inhibition of p38 MAPK sensitizes tumour cells to cisplatin-induced apoptosis mediated by reactive oxygen species and JNK. EMBO Mol Med 5: 1759-1774, 2013.
46. Lu J and Yu M and Li J: PKC-δ promotes IL-1β-induced apoptosis of rat chondrocytes and via activating JNK and P38 MAPK pathways. Cartilage: 19476035231181446, 2023 (Epub ahead of print).
47. Zhao Q, Yu M, Li J, Guo Y, Wang Z, Hu K, Xu F, Liu Y, Li L, Wan D, *et al*: GLUD1 inhibits hepatocellular carcinoma progression via ROS-mediated p38/JNK MAPK pathway activation and mitochondrial apoptosis. Discov Oncol 15: 8, 2024.
48. Wang X, Tan X, Zhang J, Wu J and Shi H: The emerging roles of MAPK-AMPK in ferroptosis regulatory network. Cell Commun Signal 21: 200, 2023.

Copyright © 2024 Jin et al. This work is licensed under a Creative Commons Attribution 4.0 International (CC BY-NC 4.0) License